Chapter 14

Imaging Systems Analysis

Overview: In this chapter we discuss a fundamental area of application involving *imaging systems.* Of course, this application area is far more encompassing than our cursory treatment here. Imaging systems are typically classified as passive or active. A *passive system* is one that is based on receiving emitted radiation by the target (e.g., blackbody radiation), or reflected radiation by the target from natural sources (e.g., reflected sunlight or moonlight). An *active system* refers to one in which the target is intentionally illuminated by a source such as a laser. Our treatment here is primarily for active systems.

A *coherent imaging system* is one in which the illumination wave and reflected wave are both coherent radiation. Such imaging systems are linear with respect to the optical electromagnetic field and can therefore be analyzed by conventional linear shift-invariant (LSI) principles, which involve the notions of *impulse response* and *transfer function.* In the open atmosphere a coherent illumination wave will suffer irradiance and phase distortions, leading to a partially coherent beam. Even in the partially coherent case, the imaging system is called an *incoherent imaging system.* Incoherent systems are linear with respect to irradiance instead of optical field. The useful parameters in this case are the *point spread function* (PSF) and *optical transfer function* (OTF), which are related through two-dimensional Fourier transforms. The modulus of the OTF, known as the *modulation transfer function* (MTF), is used to describe image quality whereas the *phase transfer function* (PTF) determines image position and orientation.

Adaptive optics (AO) methods are commonly used to improve images. Imaging performance measures of an AO system, such as *resolution* and *Strehl ratio*, are defined in terms of the PSF or MTF. These particular metrics involve *Fried's atmospheric coherence width*, also known as the "seeing parameter." In the use of a beacon or guide star, the *isoplanatic angle* arises as another important parameter that describes the useable field of view.

14.1 Introduction

Electromagnetic wave absorption and scattering give rise to attenuation of the irradiance that affects the quality of images propagating through the atmosphere because of reduced contrast and image blurring of detail. Intensity and phase fluctuations due to atmospheric turbulence can also cause blurring, image jitter, and other effects that limit the practical utilization of optical instruments for astronomy and remote sensing. Image blurring is caused by a dephasing of the fringes that make up the intensity distribution. That is, when the fringes no longer add up in a coherent (in-phase) manner, the resulting image is blurred.

It has long been known (since the time of Newton) that atmospheric turbulence is deleterious to the "seeing" ability of astronomers using a ground-based telescope [1,2]. For example, if light propagating through the atmosphere from a distant source is subsequently collected by a lens of diameter D_G and brought to a focus, the quality of the image formed in the focal plane (image plane) may be greatly degraded by atmospheric turbulence. In a vacuum, the far-field diffraction pattern has an angular extent (*seeing angle*) of roughly λ/D_G, whereas in turbulence the seeing angle is λ/r_0, where r_0 is the *atmospheric coherence width* defined below. At sea level, the atmospheric coherence width is roughly $2-30$ cm at visible and IR wavelengths. Thus, although large telescopes on the order of meters in diameter permit dim objects to be observed, their achieved angular resolution is only equivalent to that obtained with a much smaller telescope on the order of centimeters (e.g., $10-30$ cm) in diameter.

Image degradation effects, such as image blurring and image dancing (jitter), are associated primarily with phase fluctuations, which are dominated by large turbulent eddies. *Image dancing* arises from the overall tilt imparted to the optical wave front by the advection of large eddies, which subsequently causes the image to move or "dance" in the focal plane as the large eddies move across the aperture (see Section 6.5). Long-term *image blur* is caused by a superposition of small-scale effects and large-scale image jitter, and thus includes effects from all scale sizes. The problem of imaging through the atmosphere is mathematically similar to the problem of beam propagation through the atmosphere. For example, beam spreading and beam wander are the beam counterparts to image resolution (or image blur) and image dancing.

Many of the deleterious effects of atmospheric turbulence on imaging systems were recognized by astronomers during the 1950s, but the basic underlying physics wasn't understood until the 1960s and later. A good review of the astronomical problem up until 1980 is provided by Roddier [2]. A more recent series of papers by Dravens et al. [3] specifically addresses atmospheric intensity scintillation of stars. Because of the effects of atmospheric turbulence on imaging, compensation methods are of great importance in imaging applications. Techniques developed over the years to mitigate these atmospheric effects include the following [4,5]:

- *Postprocessing techniques:* The first efforts to overcome atmospheric effects relied on postdetection processing of *short-exposure images* measured through turbulence. The term "short-exposure images" refers to images whose exposure time essentially "freezes the atmosphere," i.e., typically on the order of milliseconds. Such techniques, now referred to as *speckle imaging* in reference to the "speckled" appearance of the images (depicting high spatial frequency content), are aimed at estimating the modulus and phase of the Fourier transform of the object being imaged.
- *Adaptive optics methods:* Systems that use mechanical means to sense and correct for atmospherically induced wave front deformations in real time are called adaptive optics systems. The major components of an adaptive optics imaging (AOI) system are a *deformable mirror, wave front sensor*, and an *actuator command computer.* Among others, limiting factors that prevent AOI systems from achieving ideal performance are finite light levels in the wave front sensor and differences between the sensed wave front and that of the object being imaged (anisoplanatism [6]).
- *Hybrid imaging techniques:* Since neither speckle imaging nor adaptive optics are capable of completely overcoming the effects of atmospheric turbulence, other methods that combine postprocessing and adaptive optics techniques are sometimes used. These hybrid techniques provide a trade-off between predetection and postdetection methods, using the best performance features of each type of system.

The analysis of *linear shift-invariant systems* (LSI) that is so well known in the temporal-frequency study of electric circuits and other areas of engineering can also be applied to many *electro-optical* (EO) systems. In particular, it can be

applied to certain EO imaging systems except the time analysis is replaced by a two-dimensional spatial domain and the frequency domain is replaced by a wave number (spatial frequency) domain, the latter having units of *cycles per meter* (or cycles per millimeter). The notion of shift-invariance in a temporal field implies that a shift in time of the input function yields a similar shift in time of the output function. Shift-invariance in an optical system implies a *spatial shift* rather than a time shift. Specifically, this means that the input at one point in the field of view (FOV) produces a response that is identical to that of the same input at a different point in the FOV, except shifted in position. The FOV is an important design parameter of an EO system that describes the angular space in which the system accepts light. However, the performance of an optical system "on the optical axis" is usually better than that "off the optical axis." Thus, to assume the EO system is shift-invariant is generally considered only a first-order approximation, i.e., the system is shift-invariant only near the optical axis in the FOV. Nonetheless, if an optical system is (approximately) shift-invariant, we can then characterize it within its FOV at a single location.

14.2 Coherent Imaging Systems

A *coherent imaging systems* is one in which the illumination beam is spatially coherent [7–10]. However, imaging laser radars (ladar) that provide their own illumination have an advantage over passive imaging devices that must rely on natural sources of illumination or on radiation from the target itself. The use of ladar seekers for autonomous vehicle identification and targeting from short-range expendable munitions has seen an increase of interest due to the inherently high resolution (target) shape data and the relatively low cost of the sensor [11]. A number of exploratory programs over the last decade or so have proven the value of ladar for tactical applications.

14.2.1 Impulse response and coherent transfer function

Both temporal and EO systems are characterized by the impulse response function and its Fourier transform called the system transfer function. Let us assume the input function to an EO system is a *point source* on the optical axis described by

$$U_0(\mathbf{s}, 0) = \delta(\mathbf{s}). \tag{1}$$

The substitution of (1) into the *generalized Huygens-Fresnel integral* (see Section 4.9)

$$\begin{aligned} U_0(\mathbf{r}, L) &= -\frac{ik}{2\pi B}\exp(ikL)\int\int_{-\infty}^{\infty} d^2 s U_0(\mathbf{s}, 0)\exp\left[\frac{ik}{2B}(As^2 - 2\mathbf{s}\cdot\mathbf{r} + Dr^2)\right] \\ &= \int\int_{-\infty}^{\infty} d^2 s U_0(\mathbf{s}, 0) h(\mathbf{s}, \mathbf{r}), \end{aligned} \tag{2}$$

leads to the result

$$U_0(\mathbf{r}, L) = h(0, \mathbf{r}) = -\frac{ik}{2\pi B}\exp\left(ikL + \frac{ikDr^2}{2B}\right). \tag{3}$$

The function $h(0, \mathbf{r})$ is the *impulse response function* for free-space propagation. We can interpret the quantity (3) as a Gaussian-beam wave under the paraxial approximation that reduces to a spherical wave in the absence of optical elements (i.e., $B = L$ and $D = 1$).

To derive the associated transfer function for free-space propagation, we use the two-dimensional Fourier transform defined by

$$H(\nu) = \mathscr{F}^{(2)}\{h(0, \mathbf{r})\} = \int\int_{-\infty}^{\infty} e^{-2\pi i \mathbf{r}\cdot\nu} h(0, \mathbf{r})\, d^2 r, \tag{4}$$

where $\nu = (\nu_x, \nu_y)$ is a two-dimensional spatial frequency vector. Substituting Eq. (3) into (4), and dividing by $H(0)$ to normalize the expression, we obtain the *coherent transfer function* (CTF)

$$\hat{H}(\nu) = \frac{H(\nu)}{H(0)} = \exp\left(-\frac{2\pi^2 iB\nu^2}{kD}\right), \tag{5}$$

where $\nu = (\nu_x^2 + \nu_y^2)^{1/2}$ is the magnitude of the spatial frequency vector.

To take a specific case, let us consider the EO system illustrated in Fig. 14.1 for a single Gaussian lens in which the total path length from input plane to output plane is $L + L_f$. If we let W_G and F_G denote the effective lens radius and focal length, respectively, then from the *ABCD* matrix approach we have that

$$\begin{aligned}\begin{pmatrix} A & B \\ C & D \end{pmatrix} &= \begin{pmatrix} 1 & L_f \\ 0 & 1 \end{pmatrix}\begin{pmatrix} 1 & 0 \\ i\alpha_G & 1 \end{pmatrix}\begin{pmatrix} 1 & L \\ 0 & 1 \end{pmatrix} \\ &= \begin{pmatrix} 1 + i\alpha_G L_f & L + L_f(1 + i\alpha_G L) \\ i\alpha_G & 1 + i\alpha_G L \end{pmatrix},\end{aligned} \tag{6}$$

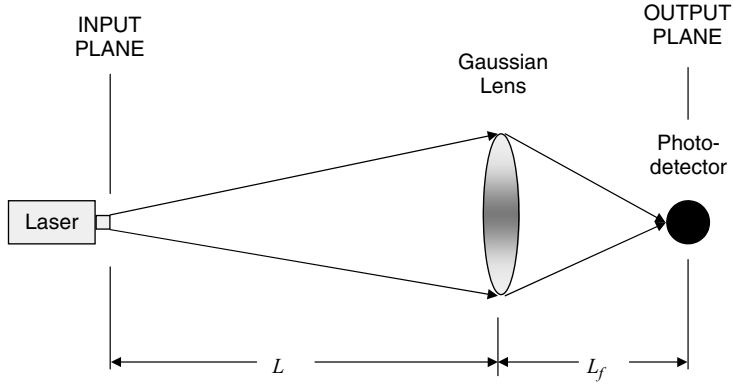

Figure 14.1 Propagation geometry for a point source originating at distance L to the left of a thin Gaussian lens of real focal length F_G and effective transmission radius W_G.

where

$$\alpha_G = \frac{2}{kW_G^2} + i\frac{1}{F_G}. \tag{7}$$

Using the matrix elements B and D identified in (6), we first simplify them to find

$$\begin{aligned} B &= L_f\left(1 + \frac{L}{L_f} - \frac{L}{F_G} + i\Omega_G\right), \\ D &= 1 - \frac{L}{F_G} + i\Omega_G, \end{aligned} \tag{8}$$

where $\Omega_G = 2L/kW_G^2$ characterizes the finite size of the lens. From (8) we deduce that the impulse response function (3) can be expressed as

$$\begin{aligned} h(0,\mathbf{r}) = &-\frac{k}{2\pi L}(\Lambda_2 + i\Theta_2)\exp[ik(L+L_f)] \\ &\times \exp\left\{-\left[\Theta_2\Omega_G - \Lambda_2\left(1 - \frac{L}{F_G}\right)\right]\frac{kr^2}{2L} + i\left[\Theta_2\left(1 - \frac{L}{F_G}\right) + \Lambda_2\Omega_G\right]\frac{kr^2}{2L}\right\}, \end{aligned} \tag{9}$$

where

$$\begin{aligned} \Theta_2 &= \frac{L}{L_f}\left[\frac{1 + L/L_f - L/F_G}{(1 + L/L_f - L/F_G)^2 + \Omega_G^2}\right], \\ \Lambda_2 &= \frac{L}{L_f}\left[\frac{\Omega_G}{(1 + L/L_f - L/F_G)^2 + \Omega_G^2}\right]. \end{aligned} \tag{10}$$

For an imaging system the distances L and L_f are related to the focal length F_G of the lens by

$$1 + \frac{L}{L_f} - \frac{L}{F_G} = 0 \tag{11}$$

Hence, we see that $\Theta_2 = 0$ and $\Lambda_2 = L/L_f\Omega_G$, which reduces (9) to

$$h(0,\mathbf{r}) = -\frac{k^2 D_G^2}{32\pi L L_f}\exp[ik(L+L_f)]\exp\left(-\frac{k^2 D_G^2 r^2}{32L_f^2} + \frac{ikr^2}{2L_f}\right), \tag{12}$$

where D_G denotes the "hard aperture" diameter of the lens for which it is conventional to equate $D_G^2 = 8W_G^2$. The associated normalized CTF in this case is the Gaussian function

$$\hat{H}(\nu) \cong \exp\left[-8\left(\frac{\lambda L_f \nu}{D_G}\right)^2\right], \tag{13}$$

where we set $k = 2\pi/\lambda$.

Equations (12) and (13) represent the impulse response function and CTF for the free-space propagation of an optical wave using an *ABCD* matrix representation for the optical elements (lens and finite aperture). If we use a hard limiting aperture instead of a Gaussian aperture model based on an *ABCD* matrix, the resulting expression for the CTF is the (circular) step function

$$\hat{H}(\nu) = \begin{cases} 1, & \nu < D_G/2\lambda L_f \\ 0, & \nu > D_G/2\lambda L_f, \end{cases} \tag{14}$$

and the corresponding expression for the impulse response function is the well-known result [12–14]

$$h(0, \mathbf{r}) = \frac{k^2 D_G^2}{8\pi L_f^2} \frac{J_1 \dfrac{kD_G r}{2L_f}}{\dfrac{kD_G r}{2L_f}}, \tag{15}$$

where $J_1(x)$ is a Bessel function of the first kind. A measure of optical system performance is based on the highest spatial frequency associated with the CTF—higher spatial frequencies mean better resolution of small features of the image. The cutoff spatial frequency given by (14) is $D_G/2\lambda L_f$, which substituted into (13) yields $e^{-2} \cong 0.135$. Because both the $1/e$ and $1/e^2$ values are commonly taken to define the effective width of a Gaussian function, the highest spatial frequency of the imaging system described by CTF model (13) (based on $1/e^2$ criterion) or (14) is the same.

To further compare the Gaussian model with the hard aperture model, we plot the magnitude of the impulse function (12) in Fig. 14.2 along with the conventional result of (15), both normalized to unity at $r = 0$. The first zero of (15) occurs at

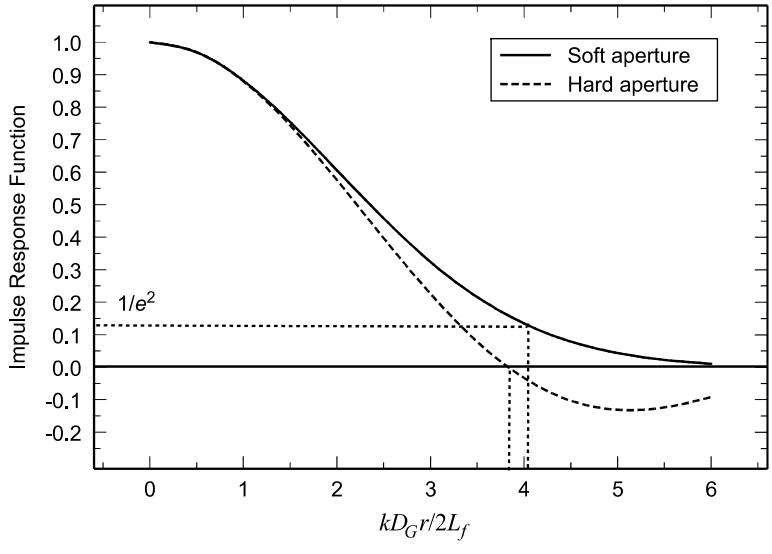

Figure 14.2 Normalized impulse response of a simple coherent imaging system.

$r = 1.22\lambda L_f/D_G$, which corresponds to the spatial resolution, whereas the $1/e^2$ value of the normalized impulse response (12) occurs at $r = 1.27\lambda L_f/D_G$, nearly the same value.

14.3 Incoherent Imaging Systems

The results given in the last section are for a coherent imaging system in the absence of atmospheric effects; that is, the object being imaged is illuminated by coherent, monochromatic light. The linear system analysis for this case is applied directly to *field* quantities, leading to the notions of impulse response function and CTF as described by Eqs. (12)–(15). An incoherent imaging system is the extreme opposite case. Most active imaging systems are neither extreme case, but generally involve partially coherent light. For example, coherent illumination of a target in the presence of atmospheric turbulence leads to a partially coherent wave. It is customary in such cases to treat the system as a completely incoherent imaging system [12–18] because of mathematical simplification.

Objects viewed by a sensor in an imaging system are broadly classified as *targets* and *backgrounds.* Targets are the objects of interest, and the backgrounds are considered to be "clutter" that interferes with recognition of the targets. Clutter includes all other radiation signals that enter the aperture of the sensor. In particular, clutter includes the background objects that are similar in size and shape to the target and, consequently, make it difficult to distinguish targets from clutter. EO systems are modeled as responding to target-to-background *contrast* based on target reflectivity and background reflectivity. In general, contrast deals with relative differences in irradiance levels ("good contrast" corresponds to large differences in irradiance levels), but various definitions of contrast are used.

EO imaging systems typically respond to wavelengths that range from 0.4 to 2 μm. In general, target radiation having a wavelength $<3-4$ μm can be attributed to radiation from sources external to the target (e.g., sun, moon, or artificial source). If the target is opaque and diffuse (most objects fall into this category), the light flux (power) viewed by an EO sensor comes from target reflections. This is in contrast with infrared systems operating in the 3–5 μm band and the 8–12 μm band in which the signals come primarily from the target and background emission of blackbody radiation.

14.3.1 Point spread function and modulation transfer function

The conventional model of an incoherent imaging system is that each field point on the object of interest is completely independent of all other field points. Thus, the system is linear with *irradiance*, not optical field, and the impulse response or *point spread function* (PSF) of an incoherent system is the irradiance in the output plane of a point source. The transfer function, which is the normalized two-dimensional Fourier transform of the PSF, is in general a complex function known as the *optical transfer function* (OTF). The magnitude of the OTF is

called the *modulation transfer function* (MTF), which basically describes image quality. The phase of the OTF is the *phase transfer function* (PTF) which determines image position and orientation. If the phase is uniform, all portions of the image are displaced by the same amount (no distortion). However, if portions of the image are displaced differently from other portions, then the image is distorted (e.g., lens aberrations). Because the OTF is the Fourier transform of a real function, it follows that the MTF is an even function and the PTF is an odd function. Of course, if the PSF is an even function, the PTF is zero.

The PSF for an EO system in free space can be deduced from Eq. (3), i.e.,

$$\begin{aligned} \mathrm{PSF}_0(\mathbf{r}) = |h(0,\mathbf{r})|^2 &= \frac{k}{4\pi^2|B|^2}\exp\left[\left(\frac{iD}{B}-\frac{iD^*}{B^*}\right)\frac{kr^2}{2}\right] \\ &= \frac{k}{4\pi^2|B|^2}\exp\left(-\frac{2r^2}{W^2}\right), \end{aligned} \tag{16}$$

where W is the spot size radius in the output plane and * denotes complex conjugate. The corresponding OTF becomes (see also Section 4.10.2)

$$\mathrm{OTF}_0(\nu) = \exp\left(-\frac{1}{2}\pi^2 W^2\nu^2\right). \tag{17}$$

Noting that the Gaussian function in the PSF (16) is real and even in distance variable r, the OTF (17) is real and even in spatial frequency ν (the PTF is zero). Moreover, the OTF is positive so it is identical with the MTF. The OTF (or MTF) given by (17) for the simple imaging system in Fig. 14.1 reduces to the form

$$\mathrm{MTF}_0(\nu) \cong \exp\left[-4\left(\frac{\lambda L_f\nu}{D_G}\right)^2\right]. \tag{18}$$

For a hard-aperture lens system, the (normalized) PSF deduced from (15) is

$$\frac{\mathrm{PSF}_0(\mathbf{r})}{\mathrm{PSF}_0(0)} = \left[\frac{J_1(\pi D_G r/\lambda L_f)}{\pi D_G r/\lambda L_f}\right]^2, \tag{19}$$

called the *Airy disk*, and the corresponding OTF (or MTF) is then [12,16,17]

$$\mathrm{MTF}_0(\nu) = \begin{cases} \dfrac{2}{\pi}\left\{\cos^{-1}\left(\dfrac{\lambda L_f\nu}{D_G}\right) - \left(\dfrac{\lambda L_f\nu}{D_G}\right)\left[1-\left(\dfrac{\lambda L_f\nu}{D_G}\right)^2\right]^{1/2}\right\}, & \nu < \dfrac{D_G}{\lambda L_f}, \\ 0, & \nu > \dfrac{D_G}{\lambda L_f}. \end{cases} \tag{20}$$

The highest (or cutoff) spatial frequency of the incoherent imaging system described by the MTF (20) is $D_G/\lambda L_f$, which when substituted into (18) yields the value $e^{-4} \cong 0.02$. For the purpose of comparing the Gaussian model with the hard-aperture model, the graphs of the respective MTFs defined by Eqs. (18) and (20) are illustrated in Fig. 14.3.

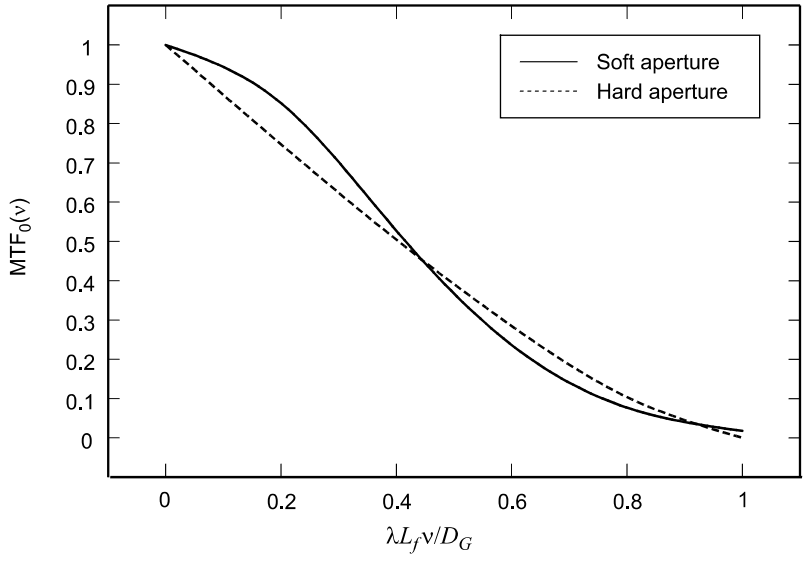

Figure 14.3 MTF for a simple imaging system with aperture diameter D_G.

14.3.2 Fried's parameter and long-term resolution

Image-degrading effects of an optical system can be described in terms of the MTF and the *long-exposure resolution.* The spatial resolution of an imaging system describes the system's ability to distinguish between two closely spaced point sources. It is regarded as a measure of system performance and is related to the width of the PSF.

To characterize atmospheric effects on the performance of an imaging system we again rely on the MTF. Knowledge of the atmospheric MTF allows the optical path in many cases to be treated as simply another cascade element in the overall system. Thus, ignoring target effects for now and concentrating on the simple imaging system illustrated in Fig. 14.1, we can write the total MTF of the propagation path up to the detector of the imaging system as the product

$$\mathrm{MTF}_{\mathrm{total}}(\nu) = \mathrm{MTF}_0(\nu)\mathrm{MTF}_{\mathrm{atm}}(\nu), \tag{21}$$

where $\mathrm{MTF}_0(\nu)$ is the MTF of the receiver optics. The atmospheric MTF is composed of two parts—that caused by aerosols along the path and that caused by optical turbulence. Although not exact, the atmospheric MTF to a first-order approximation can also be written in product form as [17]

$$\mathrm{MTF}_{\mathrm{atm}}(\nu) = \mathrm{MTF}_{\mathrm{turb}}(\nu)\mathrm{MTF}_{\mathrm{aerosol}}(\nu). \tag{22}$$

Wave absorption and scattering by the particulates of the atmosphere give rise to *attenuation* of the optical wave, thereby reducing the contrast of the final image

and possibly causing the image detail to be blurred. The "classical form" of the aerosol MTF is given by [17]

$$\mathrm{MTF}_{\mathrm{aerosol}}(\nu) = \begin{cases} \exp[-A_a L - S_a L(\nu/\nu_c)^2], & \nu < \nu_c \\ \exp[-(A_a + S_s)L], & \nu > \nu_c, \end{cases} \tag{23}$$

where A_a and S_a are absorption and scattering coefficients and ν_c is the cutoff spatial frequency. Note that for spatial frequencies exceeding the cutoff frequency, the aerosol MTF equals the atmospheric transmission τ (see Section 1.3.2). The spatial frequency cutoff is proportional to a/λ, where a is the average aerosol particle radius. For most aerosols, the radius a is comparable with wavelength. Modifications of (23) to account for imaging instrumentation limitations have been proposed by Kopeika [17] but will not be discussed here.

To obtain the long-term MTF from the *ABCD* matrix formulation based on a *spherical wave* (point source), we first determine the mean irradiance (including the effects of optical turbulence) in the image plane of the lens. This mean irradiance for the system shown in Fig. 14.1 is the PSF, which can be approximated by (see Section 10.2.4)

$$\mathrm{PSF}(\mathbf{r}) = \frac{\pi^2 D_G^4}{64\lambda^2 L_f^2[1 + (D_G/r_0)^{5/3}]} \exp\left\{ -\frac{\pi^2 D_G^2 r^2}{4\lambda^2 L_f^2[1 + (D_G/r_0)^{5/3}]} \right\}, \tag{24}$$

where $r_0 = 2.1\rho_0$. The *atmospheric coherence width* r_0 was originally introduced by Fried [1,19], who showed that it is an important measure of the performance of an imaging system. Hence, it is also widely known now as *Fried's parameter.* In the case of a spherical wave and a horizontal path in which the refractive-index structure parameter C_n^2 is essentially constant, Fried's parameter is $r_0 = (0.16 C_n^2 k^2 L)^{-3/5}$. For astronomical applications, however, Fried's parameter is usually defined for an infinite plane wave by (see also Section 12.4)

$$r_0 = \left[0.42 k^2 \int_0^L C_n^2(z)\, dz \right]^{-3/5}, \tag{25}$$

where z is propagation distance. The normalized two-dimensional Fourier transform of the PSF (24), multiplied by the aerosol MTF, leads to the total MTF given by

$$\begin{aligned} \mathrm{MTF}_{\mathrm{total}}(\nu) = {} & \exp\left[-4\left(\frac{\lambda L_f \nu}{D_G} \right)^2 \right] \\ & \times \exp\left[-4\left(\frac{\lambda L_f \nu}{D_G} \right)^{1/3} \left(\frac{\lambda L_f \nu}{r_0} \right)^{5/3} \right] \mathrm{MTF}_{\mathrm{aerosol}}(\nu). \end{aligned} \tag{26}$$

The first exponential function on the right is the optics MTF (18) and the second is the turbulence MTF. In this analysis we have formally introduced the aerosol MTF by simply multiplying the transform by (23). Because high spatial

frequencies contain the fine detail of an object, imaging systems that permit high-frequency content are considered best. Thus, in the absence of atmospheric effects, Eq. (26) suggests that a large aperture (i.e., telescope diameter D_G) is best.

For the analysis involving a hard aperture it is customary to describe the MTF for a *plane wave* (rather than a point source) incident on a circular lens. Again, we assume the aperture diameter is D_G and focal length is F_G. In the focal plane of the lens, the free-space MTF is that given by (20) where we now set $L_f = F_G$. Following the analysis of Fried [1], the long-term turbulence MTF can be deduced from the formulation of the MCF in the receiver aperture plane (see Chap. 6). For the case of an incident plane wave, the *turbulence MTF* in the focal plane of the lens is

$$\begin{aligned} \mathrm{MTF}_{\mathrm{turb}}(\nu) &= \exp\left[-\left(\frac{\rho}{\rho_{\mathrm{pl}}}\right)^{5/3}\right]\Bigg|_{\rho=\lambda F_G \nu} \\ &= \exp\left[-3.44\left(\frac{\lambda F_G \nu}{r_0}\right)^{5/3}\right], \quad 1/L_0 \ll \nu \ll 1/l_0, \end{aligned} \tag{27}$$

where, as above, we see that optical turbulence acts like a low-pass filter on an optical system by filtering out the high spatial frequencies. Taking atmospheric effects into account, the total average MTF (21) of the optical system shown in Fig. 14.1 leads to

$$\begin{aligned} \mathrm{MTF}_{\mathrm{total}}(\nu) = \frac{2}{\pi}&\left\{\cos^{-1}\left(\frac{\lambda F_G \nu}{D_G}\right) - \left(\frac{\lambda F_G \nu}{D_G}\right)\left[1 - \left(\frac{\lambda F_G \nu}{D_G}\right)^2\right]^{1/2}\right\} \\ &\times \exp\left[-3.44\left(\frac{\lambda F_G \nu}{r_0}\right)^{5/3}\right]\mathrm{MTF}_{\mathrm{aerosol}}(\nu). \end{aligned} \tag{28}$$

Based on (26) or (28), we see that the resolving power is limited by the optics when the diameter D_G is smaller than r_0, and limited by the atmosphere when D_G is larger than r_0. The coherence diameter r_0 is often called the "seeing parameter" because large values of r_0 mean "good seeing" and small values mean "bad seeing."

In Fig. 14.4 we plot the MTFs (26) and (28) [not including $\mathrm{MTF}_{\mathrm{aerosol}}(\nu)$] with several values of D_G/r_0 for the sake of comparison. Here we see that the highest spatial frequency corresponding to the point where the MTF drops to 0.02 is roughly the same for each model. Although (26) is based on a spherical wave and (28) on a plane wave, we see that there is very little difference between the two expressions for the given values of D_G/r_0. For values of D_G/r_0 much greater than unity, however, the two expressions will predict somewhat different results.

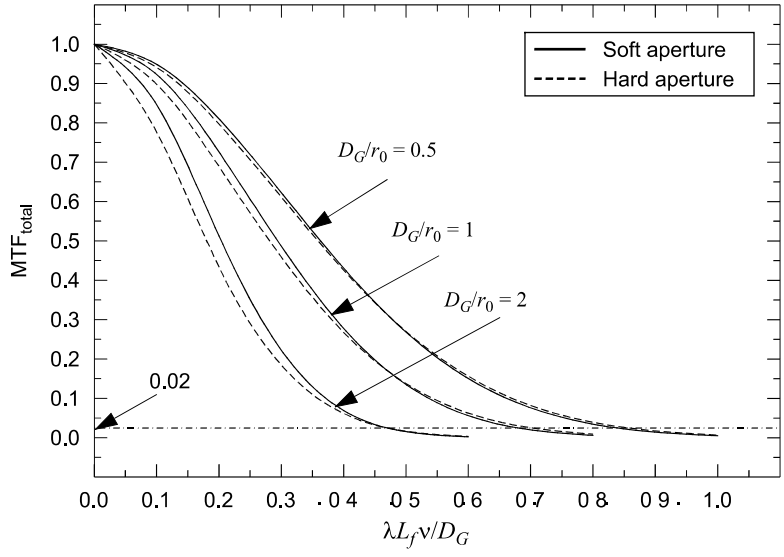

Figure 14.4 Total MTFs given by Eqs. (26) and (28) (not including $\mathrm{MTF}_{\mathrm{aerosol}}$) as a function of scaled spatial frequency. The horizontal dashed-dotted line in the graph corresponds to the point where the MTF reaches 2% of it's maximum value.

Another measure of system performance in an imaging system that takes into account the volume under the MTF surface is the *long-exposure resolution* [1]

$$\begin{aligned} R &= \int_0^{2\pi} \int_0^{D_G/\lambda F_G} \mathrm{MTF}_0(\nu)\mathrm{MTF}_{\mathrm{turb}}(\nu)\nu \, d\nu \, d\theta \\ &= \frac{4D_G^2}{\lambda^2 F_G^2} \int_0^1 u\left(\cos^{-1} u - u\sqrt{1-u^2}\right) \exp\left[-3.44\left(\frac{D_G u}{r_0}\right)^{5/3}\right] du, \end{aligned} \tag{29}$$

deduced from (28). The "limiting resolution" $R_{\max} = \pi r_0^2/4\lambda^2 F_G^2$ is the limiting value of the integral (29) as the lens diameter D_G becomes arbitrarily large. The ratio $R/R_{\max}$, shown in Fig. 14.5 as a function of D_G/r_0, can be closely approximated by

$$\frac{R}{R_{\max}} \cong \frac{(D_G/r_0)^2}{\left[1 + (D_G/r_0)^{5/3}\right]^{6/5}} \cong \begin{cases} (D_G/r_0)^2, & D_G \ll r_0, \\ 1, & D_G \gg r_0. \end{cases} \tag{30}$$

Note that the ratio $R/R_{\max}$ in Fig. 14.5 increases with aperture diameter D_G until the diameter approaches the coherence width r_0. For aperture sizes such that $D_G/r_0 > 1$, this increase is greatly curtailed and, for $D_G/r_0 \gg 1$, there is no significant further increase in resolution. The value $D_G = r_0$ is the location of the "knee" of the curve. The important deduction here is that the atmospheric-induced coherence width imposes a severe limit on the effective aperture size of the system. It is interesting that the curve in Fig. 14.5 also describes the

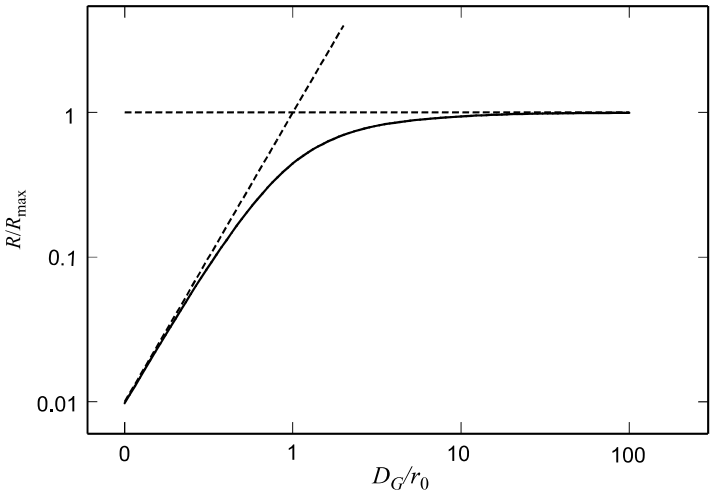

Figure 14.5 Normalized resolution in long-exposure imaging as a function of scaled aperture diameter D_G/r_0.

improvement of normalized SNR in an optical heterodyne receiver for increasing aperture diameter D_G [19].

14.3.3 Short-term modulation transfer function

The above formulation for the atmospheric turbulence MTF [Eq. (24)] is based on long-time averages and, hence, long-time exposures. Large eddies comparable in size to the receiver aperture move across the aperture at a nominal time equal to $D_G/V_\perp$, where $V_\perp$ is the mean wind speed transverse to the propagation path. Long-time averaging is determined by the time required to average over several of these largest eddies. Motion of the smallest eddies is ordinarily estimated by the inner scale size. Thus, time scales on the order of $D_G/V_\perp$ or less generally correspond to what is called the short exposure time. That is, in the case of short exposure imaging the imaging system will experience only one realization of the atmospheric fluctuations.

It was recognized early on that one of the dominant effects of atmospheric turbulence on imaging systems is random wave front tilt. Also called the angle of arrival (see Section 6.5), wave front tilt is generally modeled mathematically as the slope of the best fit plane to the incoming wave front. If we consider a long series of short exposures, a blurred image is seen that moves about the aperture (image dancing), caused by changes in the tilt induced by the large eddies. It is this random "dancing" of the image that accounts for most of the image degradation in a long exposure. The major distinction in the short exposure time is that it does not include the motion of large eddies responsible for image dancing. Thus, a short-exposure image does not see any distortion caused by the tilt. However, a single short exposure of an object yields an image that possesses

higher spatial frequencies in the form of a "speckle pattern," similar to that associated with laser light scattered from a rough surface.

The approach used by Fried [1] for the mathematical treatment of short exposures was to consider the "tilt-removed" phase of the wave front. By reciprocity (see Section 8.3), wave front tilt is similar to beam wander. Hence, based on the mean irradiance (45) in Chap. 10, we deduce that the tilt-removed (or short-term) PSF can be derived from

$$\begin{aligned} \mathrm{PSF}_{\mathrm{ST}}(\mathbf{r}) = \frac{W_G^2}{W^2}\exp\left(-\frac{2r^2}{W^2}\right)\exp\Bigg\{-4\pi^2 k^2 L\int_0^1\int_0^\infty \kappa\Phi_n(\kappa) \\ \times[1-H_{\mathrm{LS}}(\kappa,\xi)]\left[1-\exp\left(-\frac{L\kappa^2\xi^2}{k\Omega_G}\right)I_0\left(\frac{2\kappa\xi Lr}{L_f\Omega_G}\right)\right]d\kappa\, d\xi\Bigg\}, \end{aligned} \tag{31}$$

where $H_{\mathrm{LS}}(\kappa,\xi)$ is the large-scale filter function introduced in Chap. 6 for calculating beam wander of a focused beam. Adapted to wave front tilt, it has the form

$$H_{\mathrm{LS}}(\kappa,\xi) = \exp\left(-\kappa^2 W_G^2\xi^2\right) = \exp\left(-\frac{2L\kappa^2\xi^2}{k\Omega_G}\right). \tag{32}$$

The evaluation of (31) with the filter function (32) yields

$$\mathrm{PSF}_{\mathrm{ST}}(\mathbf{r}) = \frac{\pi^2 D_G^4}{64\lambda^2 L_f^2[1+0.28(D_G/r_0)^{5/3}]}\exp\left\{-\frac{\pi^2 D_G^2 r^2}{4\lambda^2 L_f^2[1+0.28(D_G/r_0)^{5/3}]}\right\}, \tag{33}$$

which differs from the long-term PSF (24) by only the coefficient in front of the ratio $(D_G/r_0)^{5/3}$. If we now take the two-dimensional Fourier transform of (33), we are led to the long-term MTF with tilt removed (which is often called the *short-term MTF*)

$$\begin{aligned} \mathrm{MTF}_{\mathrm{ST}}(\nu) &= \mathrm{MTF}_0(\nu)\mathrm{MTF}_{\mathrm{ST,\,turb}}(\nu) \\ &= \exp\left[-4\left(\frac{\lambda L_f\nu}{D_G}\right)^2\right]\exp\left[-1.12\left(\frac{\lambda L_f\nu}{D_G}\right)^{1/3}\left(\frac{\lambda L_f\nu}{r_0}\right)^{5/3}\right]. \end{aligned} \tag{34}$$

Once again, the first exponential function in (34) on the right-hand side is the free-space MTF, depicting that due only to the optics of the receiver system. In comparing (34) with the long-term MTF (26), we note that the smaller coefficient in the second exponential function in (34) leads to higher spatial frequencies in the short-term MTF for $D_G > r_0$, and, consequently, better resolution.

In Fried's analysis [1], he modified the long-term turbulence MTF (27) by considering the equivalent expression with tilt removed, i.e.,

$$\mathrm{MTF}_{\mathrm{ST,\,turb}}(\nu) = \exp\left\{-3.44\left(\frac{\lambda F_G\nu}{r_0}\right)^{5/3}\left[1-b\left(\frac{\lambda F_G\nu}{D_G}\right)^{1/3}\right]\right\}, \tag{35}$$

where $b = 1$ in the near field (plane wave) and $b = 0.5$ in the far field (spherical wave). If $D_G > r_0$, the additional factor in (35) resulting from the shorter time scale permits higher spatial frequencies than allowed by the long-term MTF (27).

14.3.4 Isoplanatism and the Greenwood time constant

In adaptive optics compensating imaging systems, the isoplanatic angle arises as another important parameter [5]. The principle behind adaptive optics systems is to sense the phase distortions of a known source and apply a "corrective" or conjugate phase to the outgoing beam or incoming image. A *beacon* or *laser guide star* (i.e., reference source) is often used to sense the atmospheric phase distortion, but the location of the beacon or guide star may be in a direction different from the propagation path of the object being imaged. If the angle θ between the beacon direction and the propagation path to the object is too large, proper compensation will not be achieved. The usable field of view in such cases identifies the *isoplanatic angle* θ_0, which represents an angular radius from the beacon in which the turbulence subtends a single turbulence realization.

Like r_0, the effect of isoplanatism can be formulated in terms of the MTF. In particular, the isoplanatic angle θ_0 is the $1/e$ point of the turbulence MTF defined by

$$\mathrm{MTF}_\theta(\theta) = \exp\left[-\left(\frac{\theta}{\theta_0}\right)^{5/3}\right], \tag{36}$$

which is deduced from the spherical wave MCF by setting $\rho = L\theta$. The implied isoplanatic angle is therefore

$$\theta_0 = \left[2.91k^2 \int_0^L C_n^2(z) z^{5/3} dz\right]^{-3/5}. \tag{37}$$

Typical values for θ_0 deduced from (37) at wavelength $\lambda = 0.5\,\mu\mathrm{m}$ are roughly $7-10\ \mu\mathrm{rad}$ for a near vertical path from Earth to space.

Greenwood [20] investigated the effects of finite bandwidth controllers on AO imaging system performance and developed the definition of a characteristic atmospheric frequency, now called the *Greenwood frequency*. The associated *Greenwood time constant* τ_0 specifies the time interval over which turbulence remains essentially unchanged, i.e.,

$$\tau_0 = \left[2.91k^2 \int_0^L C_n^2(z) V^{5/3}(z)\, dz\right]^{-3/5}, \tag{38}$$

where $V(z)$ is the transverse wind velocity (speed) as a function of propagation distance. For constant wind speed $V_\perp$, the time constant (38) can be directly related to Fried's parameter by

$$\tau_0 = \frac{0.32 r_0}{V_\perp}. \tag{39}$$

The time constant (39) is typically on the order of milliseconds, and the Greenwood frequency is simply the reciprocal of the time constant.

14.3.5 Strehl ratio

The *Strehl ratio* is considered another measure of performance of an adaptive-optics system. We investigated the Strehl ratio in Section 10.2.4 for the optical system shown in Fig. 14.1 with a point source at the transmitter. Fundamentally, the Strehl ratio is defined by the ratio of the peak focal-plane mean irradiance in the presence of atmospheric turbulence to the peak focal-plane free-space irradiance. Consequently, using the *ABCD* ray matrix representation of the optical system, the Strehl ratio can be inferred from the PSFs (16) and (24). Thus, under weak irradiance fluctuations, we have

$$\mathrm{SR} = \frac{\mathrm{PSF}(0)}{\mathrm{PSF}_0(0)} = \frac{1}{1 + (D_G/r_0)^{5/3}}, \quad D_G/r_0 \ll 1. \tag{40}$$

Values of the Strehl ratio close to unity are considered best for imaging. Note that the short-term Strehl ratio deduced from (33) has a coefficient of 0.28 in front of the factor $(D_G/r_0)^{5/3}$ instead of unity, leading to a better Strehl ratio. Under more general conditions, it can be shown that the long-term Strehl ratio is defined by [1]

$$\mathrm{SR} = \frac{16}{\pi}\int_0^1 u\left(\cos^{-1} u - u\sqrt{1-u^2}\right)\exp\left[-3.44\left(\frac{D_G u}{r_0}\right)^{5/3}\right] du, \tag{41}$$

which is similar to the long-exposure resolution given by (29). Although the exact evaluation of this expression is difficult, it can be closely approximated by the simple algebraic function

$$\mathrm{SR} \cong \frac{1}{[1 + (D_G/r_0)^{5/3}]^{6/5}}. \tag{42}$$

The approximation (42) is typically within 6% of the exact numerical value of (41) for values $D_G \sim r_0$, and the error is considerably smaller for the asymptotic regimes $D_G/r_0 \ll 1$ and $D_G/r_0 \gg 1$. Also, under weak irradiance fluctuations in which $D_G/r_0 \ll 1$ there is little difference between (40) and (42) (see Fig. 10.5).

Sasiela [21] calculates the Strehl ratio (41) using Mellin transform techniques and his general result is expressed as a Meijer G-function [22]. In addition, he develops the asymptotic series representation

$$\mathrm{SR} = \left(\frac{r_0}{D_G}\right)^2 - 0.6159\left(\frac{r_0}{D_G}\right)^3 + 0.0500\left(\frac{r_0}{D_G}\right)^5 + \cdots, \quad \frac{D_G}{r_0} > 2. \tag{43}$$

Using only the first two terms of this expression when $D_G/r_0 > 2$ leads to a value of the Strehl ratio that has an error of $<1\%$.

14.4 Laser Imaging Radar

The development of *laser imaging radar* (ladar) has led to many technical options for a variety of target detection and imaging scenarios [23,24]. However, such systems are subject to atmospheric effects that make it more difficult to obtain a good image of the target. Moreover, when the target is rough and larger than the correlation width of the laser illumination, scintillation presents itself as a speckling of the target illumination. The combination of surface-created speckle and atmospheric scintillation can present serious limitations to all imaging systems.

In our analysis of a laser imaging radar we will assume the exit/entrance optics of the radar has an unobscured circular pupil of diameter D_G, and the received waveform is subsequently imaged onto a detector array for signal processing. In general, the target of interest may have both *specular* (glint) and *diffuse* (speckle) reflection components. However, we only consider cases where the target is a small unresolved specular (glint) object.

14.4.1 MTF of return wave from an unresolved small target

The characteristics of the returning optical wave reflected from a target contain information about the target that is distorted by atmospheric conditions, including aerosol absorption and scattering effects. In our analysis we consider the case of a small unresolved glint target in which the transceiver is in the far field of the target. This type of target is commonly called a *point target.* We assume in this case that surface-generated speckle does not appear in the echo wave.

The total MTF is determined from (*i*) the optics of the receiver, (*ii*) the aerosol effects, and (*iii*) the MCF of the return beam from the target. A simple model for the MTF of the receiver optics is given by Eq. (18), which we now express in the form

$$\mathrm{MTF}_0(\nu_a) = \exp\left[-4\left(\frac{\lambda \nu_a}{D_G}\right)^2\right], \tag{44}$$

where ν_a is angular spatial frequency. To account for the double-passage propagation path of length $2L$, the aerosol MTF (23) for angular frequencies greater than the cutoff frequency associated with the average particle size can be expressed by

$$\mathrm{MTF}_{\mathrm{aerosol}}(\nu_a) = \exp\left(-2A_aL - 2S_aL\right), \quad \nu_a > \nu_{ac}, \tag{45}$$

where $\nu_{ac} \sim a/\lambda$ is the cutoff angular frequency. For a sufficiently small target, the turbulence MTF of the echo beam is that associated with a returning spherical wave (see Chap. 13). Thus, the turbulence MTF takes the form

$$\mathrm{MTF}_{\mathrm{turb}}(\nu_a) = \exp\left[-3.44\left(\frac{\lambda \nu_a}{r_0}\right)^{5/3}\right], \tag{46}$$

where r_0 is the atmospheric coherence diameter of the return spherical wave defined along a horizontal path by

$$r_0 = (0.16C_n^2 k^2 L)^{-3/5}, \quad l_0 \ll r_0 \ll L_0. \tag{47}$$

The total MTF of the propagation path is roughly the product of MTFs (44)–(46).

14.4.2 Single pixel scintillation index of return wave

Here we introduce models for the scintillation index of the return beam for a single pixel in the image plane of the collecting lens. Such knowledge is important in determining the system signal-to-noise ratio (SNR) and the probability of dropouts associated with atmospheric turbulence effects.

Under weak fluctuation conditions, the double-passage scintillation index in the image plane of a *bistatic system* associated with a transmitted *spherical wave* is given by (see Chap. 13)

$$\sigma_I^2(D_G, 2L + L_f)_{\text{bistatic}} = \sigma_i^2(0) + \sigma_E^2(D_G), \tag{48}$$

where $\sigma_i^2(0)$ is identified with the incident spherical wave and $\sigma_E^2(D_G)$ is identified with the aperture-averaged reflected (echo) wave for a collecting aperture D_G associated with a single pixel. Based on *weak fluctuation theory*, these expressions are given by

$$\sigma_i^2(0) \cong \sigma_{\ln i}^2(0) = 8\pi^2 k^2 L \int_0^1 \int_0^\infty \kappa \Phi_n(\kappa) \left\{ 1 - \cos\left[\frac{L\kappa^2}{k} \xi(1-\xi) \right] \right\} d\kappa \, d\xi, \tag{49}$$

$$\sigma_E^2(D_G) \cong \sigma_{\ln E}^2(D_G) = 8\pi^2 k^2 L \int_0^1 \int_0^\infty \kappa \Phi_n(\kappa) \exp\left(-\frac{D_G^2 \kappa^2 \xi^2}{16} \right) \times \left\{ 1 - \cos\left[\frac{L\kappa^2}{k} \xi(1-\xi) \right] \right\} d\kappa \, d\xi. \tag{50}$$

We recognize Eq. (49) as the scintillation index of a spherical wave that has propagated a distance L in one direction, and Eq. (50) is the same except for the aperture averaging effect caused by the receiver collecting lens. By utilizing previous expressions developed in Chaps. 9 and 10, the double-passage scintillation index (48) under *weak-to-strong fluctuations* takes the form (ignoring inner scale and outer scale effects)

$$\sigma_I^2(D_G, 2L + L_f)_{\text{bistatic}} = \exp[\sigma_{\ln i}^2(0) + \sigma_{\ln E}^2(D_G)] - 1$$

$$= \exp\left[\frac{0.49\beta_0^2}{\left(1 + 0.56\beta_0^{12/5}\right)^{7/6}} + \frac{0.51\beta_0^2}{\left(1 + 0.69\beta_0^{12/5}\right)^{5/6}} + \frac{0.49\beta_0^2}{\left(1 + 0.18d_G^2 + 0.56\beta_0^{12/5}\right)^{7/6}} + \frac{0.51\beta_0^2\left(1 + 0.69\beta_0^{12/5}\right)^{-5/6}}{1 + 0.90d_G^2 + 0.62d_G^2\beta_0^{12/5}}\right] - 1, \quad (51)$$

where $d_G = (kD_G^2/4L)^{1/2}$ and $\beta_0^2 = 0.5C_n^2k^{7/6}L^{11/6}$.

In Fig. 14.6 we plot Eq. (51) as a function of β_0 for an equivalent aperture size D_G associated with a single pixel as seen at the input collecting aperture. Equivalent aperture sizes $D_G = 5, 10$ mm, and $D_G \ll 1$ mm are shown as well as the limiting case of a very large collecting aperture (i.e., the scintillation index of a single-pass wave)

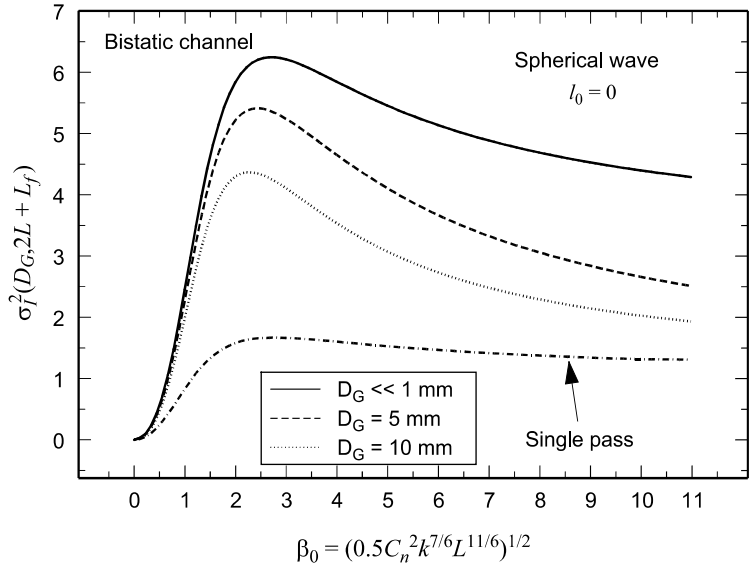

Figure 14.6 Scintillation index of a spherical wave in the image plane as a function of β_0 for various size collecting apertures for a single pixel. The single-pass curve represents the residual scintillation for an infinitely large aperture.

$$\lim_{D_G \to \infty} \sigma_I^2(D_G, 2L + L_f)_{\text{bistatic}}$$

$$= \exp\left[\frac{0.49\beta_0^2}{\left(1 + 0.56\beta_0^{12/5}\right)^{7/6}} + \frac{0.51\beta_0^2}{\left(1 + 0.69\beta_0^{12/5}\right)^{5/6}}\right] - 1. \tag{52}$$

That is, there is a residual scintillation associated with (51) that cannot be further reduced through aperture averaging.

For a *monostatic system* under weak fluctuations, we have

$$\sigma_I^2(D_G, 2L + L_f)_{\text{monostatic}} = \sigma_i^2(0) + \sigma_E^2(D_G) + 2\sigma_{iE}^2(D_G), \tag{53}$$

where the first two terms are defined by (49) and (50), and the third term, caused by correlations between the incident and echo waves, is given by (see Chap. 13)

$$\sigma_{iE}^2(D_G) \cong \sigma_{\ln iE}^2(D_G) = 8\pi^2 k^2 L \int_0^1 \int_0^\infty \kappa \Phi_n(\kappa) \exp\left(-\frac{D_G^2 \kappa^2 \xi^2}{32}\right)$$
$$\times \left\{1 - \cos\left[\frac{L\kappa^2}{k}\xi(1 - \xi)\right]\right\} d\kappa\, d\xi. \tag{54}$$

Note that (54) has the same form as (50) except for the factor 32 in the denominator of the first exponential function in place of 16. Extension of (54) into moderate-to-strong fluctuation regimes remains an open problem.

14.4.3 Single pixel signal-to-noise ratio

In this section we briefly examine the mean SNR associated with a single pixel of a detection array that is shot-noise limited. Understanding single pixel performance is essential to understanding overall image quality. In general, scintillation in the reflected waveform at the receiver can severely limit the single pulse image SNR. To compensate for this, some sort of multiframe averaging will generally be required to achieve satisfactory image quality [23].

Reduced scintillation caused by aperture averaging takes place when the collecting aperture of the receiver lens is larger than the correlation width of the incident radiation. In a direct detection system with equivalent collecting aperture D_G for a single pixel, the mean SNR for a single pixel is given by [25]

$$\langle \text{SNR} \rangle = \frac{\text{SNR}_0}{\sqrt{\dfrac{P_{S0}}{\langle P_S \rangle} + \sigma_I^2(D_G, 2L + L_f)\text{SNR}_0^2}}. \tag{55}$$

Here, $\sigma_I^2(D_G, 2L + L_f)$ is the flux variance defined above, SNR_0 is the SNR in the absence of optical turbulence, and P_{S0} is the signal power in the absence of turbulence effects. The power ratio $P_{S0}/\langle P_S \rangle$, which provides a measure of SNR

deterioration caused by atmospheric-induced beam spreading, is simply the ratio of spot sizes in turbulence and in free space. For a point source, $P_{S0}/\langle P_S\rangle = 1$, but for a Gaussian-beam wave reflected from the target we have

$$\frac{P_{S0}}{\langle P_S\rangle} = (1 + 1.63\sigma_R^{12/5}\Lambda_1). \tag{56}$$

14.5 Zernike Polynomials

In analyzing the effects of turbulence on an imaging system, it is advantageous to represent the phase of the corrupted optical wave in a series of simple orthogonal functions. This approach was first used in the description of fixed aberrations where the phase was expanded using the lower-order Zernike polynomials [15].

The *Zernike polynomials* as introduced by Noll [26] represent a set of functions of two variables that are orthogonal over a circle with unit radius. It is customary to define these polynomials as a product of two functions, one depending only on a radial coordinate r and the other depending only on the angular coordinate θ, i.e.,

$$Z_n^m(r,\theta) = R_n^m(r)e^{im\theta}, \tag{57}$$

where both m and n are integers, $n \geq 0$, $-n \leq m \leq n$, and $n \pm |m|$ is even. The radial polynomial $R_n^m(r)$ is a special case of Jacobi or hypergeometric polynomial that is normalized so that $R_n^m(1) = 1$. It is defined in general by

$$R_n^m(r) = \sum_{k=0}^{(n-|m|)/2} \frac{(-1)^k(n-k)!}{\left(\frac{n+m}{2}-k\right)!\left(\frac{n-m}{2}-k\right)!}\frac{r^{n-2k}}{k!}. \tag{58}$$

Clearly, the polynomial (58) has degree n and contains no power of r less than $|m|$, where m is the angular dependence. Also, the polynomial is even if m is even and odd if m is odd. The *orthogonality* property of these polynomials is

$$\int_0^1\int_0^{2\pi} Z_n^m(r,\theta)Z_k^{m*}(r,\theta)\,r\,d\theta\,dr = \frac{\pi}{n+1}\delta_{nk} = \begin{cases} \pi/(n+1), & k = n \\ 0, & k \neq n \end{cases} \tag{59}$$

where $*$ denotes complex conjugate, and δ_{nk} is the Kronecker delta defined by $\delta_{nk} = 0$ $(k \neq n)$ and $\delta_{nk} = 1$ $(k = n)$.

14.5.1 Application in optics

One of the principal uses of the Zernike polynomials is to represent fixed aberrations in optical systems in the form of a generalized Fourier series in Zernike polynomials. Lower-order Zernike polynomials are then referred to by such names as *piston*, *tilt*, *focus*, *astigmatism*, *coma*, and so forth. By the use of these polynomials, researchers have been able to study how aberrations affect various imaging systems. They are also useful in adaptive optics systems designed for atmospheric turbulence decomposition [18,23,27].

Virtually any realistic wave front $\Phi(r,\theta)$ can be represented in a two-dimensional series of Zernike polynomials by one of the following expressions:

$$\Phi(r,\theta)=\sum_{n=0}^{\infty}\sum_{m=-n}^{n}C_{mn}R_n^m(r)e^{im\theta}, \tag{60}$$

or, alternatively,

$$\begin{aligned}\Phi(r,\theta)=A_{00}+\frac{1}{\sqrt{2}}\sum_{n=2}^{\infty}A_{0n}R_n^0(r)\\ +\sum_{n=0}^{\infty}\sum_{m=1}^{n}(A_{mn}\cos m\theta+B_{mn}\sin m\theta)R_n^m(r).\end{aligned} \tag{61}$$

The factor $1/\sqrt{2}$ is often introduced in the second term in (61) because it simplifies the final formulas for the Fourier coefficients. The Fourier coefficients in (61) are related to those in (60) by

$$\begin{aligned}A_{00}&=C_{00}, & A_{0n}&=\sqrt{2}C_{0n},\\ A_{mn}&=\frac{1}{2}(C_{mn}-iC_{-mn}), & B_{mn}&=\frac{1}{2i}(C_{mn}+iC_{-mn}).\end{aligned} \tag{62}$$

To obtain the Fourier coefficients in (60), we first multiply both sides of the expression by $rR_k^{|m|}(r)e^{-im\theta}$ and then integrate over the unit disk. This action leads to

$$\begin{aligned}\int_0^1\int_0^{2\pi}r\,\Phi(r,\theta)R_k^{|m|}(r)e^{-im\theta}\,d\theta\,dr&=\sum_{n=0}^{\infty}\sum_{m=-n}^{n}C_{mn}\int_0^1\int_0^{2\pi}rR_n^{|m|}(r)R_k^{|m|}(r)\,d\theta\,dr\\ &=\frac{\pi}{k+1}\sum_{m=-k}^{k}C_{mk}.\end{aligned} \tag{63}$$

For $k=0$, we obtain the coefficient for the piston term given by

$$C_{00}=\frac{1}{\pi}\int_0^1\int_0^{2\pi}r\Phi(r,\theta)\,d\theta\,dr=\langle\Phi(r,\theta)\rangle. \tag{64}$$

That is, this coefficient is simply the average value of the wave front $\langle\Phi(r,\theta)\rangle$. Similarly, the coefficient for focus is deduced by setting $k=2$ and $m=0$, which gives us

$$C_{02}=\frac{3}{\pi}\int_0^1\int_0^{2\pi}r(2r^2-1)\Phi(r,\theta)\,d\theta\,dr. \tag{65}$$

A useful property of the Zernike series (60) [or (61)] is that the root-mean-square (rms) wave front error due to primary (lower-order) aberrations can readily be calculated. That is, if all the Fourier coefficients in (60) are known, the geometric sum of the nonpiston terms yields the wave front variance (or "mean-square" deformation)

$$(\Delta\Phi)^2 = \frac{1}{\pi}\int_0^1\int_0^{2\pi} r[\Phi(r,\theta) - \langle\Phi(r,\theta)\rangle]^2 d\theta\, dr = \sum_{n=1}^{\infty}\sum_{m=-n}^{n}\frac{|C_{mn}|^2}{n+1}, \tag{66}$$

the square root of which gives the *rms wave front error.*

14.5.2 Atmospheric effects on imaging systems

The utility of the Zernike polynomials for analyzing the wave front of an optical wave that has passed through an imaging system with fixed aberrations has been briefly discussed in the previous section. This approach has provided a deep understanding of the lower-order aberrations on such a system. Moreover, in diagnosing the effects of atmospheric turbulence on a propagating optical wave, it can also be useful to express the turbulence-induced random phase perturbations on $\Phi(r,\theta)$ in a series of Zernike polynomials.

A modification of the Zernike polynomials (57) that is commonly used in studying atmospheric effects on imaging systems leads to Zernike functions defined by

$$\begin{aligned} Z_i(r) &\equiv Z_i[0,n] = \sqrt{n+1}R_n^0(r), \quad m = 0, \\ Z_{i,\,\text{even}}(r,\theta) &\equiv Z_{i,\,\text{even}}[m,n] = \sqrt{n+1}R_n^m(r)\sqrt{2}\cos m\theta, \quad m \neq 0, \\ Z_{i,\,\text{odd}}(r,\theta) &\equiv Z_{i,\,\text{odd}}[m,n] = \sqrt{n+1}R_n^m(r)\sqrt{2}\sin m\theta, \quad m \neq 0. \end{aligned} \tag{67}$$

The ordering scheme for these polynomials uses the rule that, for a given n, the modes with smaller m are counted first. For $m > 0$, there are two Zernike functions for each (m,n) pair as given in (67). Following this ordering scheme, we list the first few polynomials $Z_i[m,n]$ in Table 14.1. Here, the quantity $Z_1[0,0]$ represents *piston* (constant retardation or advancement of the phase over the entire beam), $Z_2[1,1]$ and $Z_3[1,1]$ represent *tilt* in the x and y directions, respectively,

Table 14.1 Table of Zernike polynomials through $(m,n) = (3,3)$.

i	m	n	Zernike polynomials $Z_i[m,n]$
1	0	0	1
2	1	1	$2r\cos\theta$
3	1	1	$2r\sin\theta$
4	0	2	$\sqrt{3}(2r^2-1)$
5	2	2	$\sqrt{6}r^2\sin 2\theta$
6	2	2	$\sqrt{6}r^2\cos 2\theta$
7	1	3	$\sqrt{8}(3r^3-2r)\sin\theta$
8	1	3	$\sqrt{8}(3r^3-2r)\cos\theta$
9	3	3	$\sqrt{8}r^3\sin 3\theta$
10	3	3	$\sqrt{8}r^3\cos 3\theta$

$Z_4[0, 2]$ is *focus* (or *defocus*), and $Z_5[2, 2]$ and $Z_6[2, 2]$ are two components of *astigmatism.*

Up to this point we have considered only the case in which the telescope aperture of the imaging system has unit radius. To account for an aperture of diameter D_G rather than of unit radius, we can simply make the change of variable $r = 2\rho/D_G$ in the above Zernike polynomials and corresponding integrals. Also, we can avoid complicated expressions like (63) for the Fourier coefficients by representing the wave front in a single series called a *modal expansion*, viz.,

$$\Phi(2\rho/D_G, \theta) = \sum_{i=1}^{\infty} a_i Z_i(2\rho/D_G, \theta). \tag{68}$$

In this case the coefficient a_i, which depends on only one index corresponding to the Zernike mode Z_i, is given by

$$a_i = \frac{4}{\pi D_G^2} \int_0^{D_G/2} \int_0^{2\pi} \rho\Phi(2\rho/D_G, \theta) Z_i(2\rho/D_G, \theta)\, d\theta\, d\rho, \quad i = 1, 2, 3, \ldots. \tag{69}$$

As an optical wave propagates through the atmosphere, small index of refraction fluctuations cause random phase perturbations on the wave front, the mean value of which is zero. In this case the coefficients a_i, $i = 1, 2, 3, \ldots$ defined by (69) are taken to be *Gaussian random variables* with zero mean, i.e.,

$$\langle a_i \rangle = \frac{4}{\pi D_G^2} \int_0^{D_G/2} \int_0^{2\pi} \rho\langle\Phi(2\rho/D_G, \theta)\rangle Z_i(2\rho/D_G, \theta)\, d\theta\, d\rho = 0. \tag{70}$$

Thus, we consider higher-order statistics of the Fourier coefficients, such as the *covariance* defined by

$$\begin{aligned} \langle a_i a_j \rangle = \left(\frac{4}{\pi D_G^2}\right)^2 \int_0^{D_G/2} \int_0^{2\pi} \int_0^{D_G} \int_0^{2\pi} \rho_1 \rho_2 C_\Phi(\rho_1, \theta_1; \rho_2, \theta_2) \\ \times Z_i(2\rho_1/D_G, \theta_1) Z_j(2\rho_2/D_G, \theta_2)\, d\theta_1\, d\rho_1\, d\theta_2\, d\rho_2, \end{aligned} \tag{71}$$

where $C_\Phi(\rho_1, \theta_1; \rho_2, \theta_2) = \langle\Phi(2\rho_1/D_G, \theta_1)\Phi(2\rho_2/D_G, \theta_2)\rangle$ is the covariance of the phase (wave front). Except for diagonal terms in which $i = j$, most other terms in (69) are zero. In particular, it has been shown that $\langle a_i a_j \rangle = 0$ for $i - j =$ odd. However, the fact that $\langle a_i a_j \rangle \neq 0$ for all $j \neq i$ means that correlation exists between some of the various Fourier coefficients. Consequently, the Zernike polynomials are not considered an "optimal basis." It has been shown that an optimal basis can be found in the form of a Karhunen-Loève series. Moreover, the orthogonal functions forming the basis of such a Karhunen-Loève series are linear combinations of the Zernike polynomials, but we will not pursue that approach here (see, for example, [3]).

Building on the above results, the mean-square phase value is defined by

$$\varepsilon^2 = \frac{4}{\pi D_G^2} \int_0^1 \int_0^{2\pi} r\langle\Phi^2(2\rho/D_G, \theta)\rangle\, d\theta\, dr = \sum_{i=1}^{\infty} \langle (a_i)^2 \rangle, \tag{72}$$

which is simply the sum of mean-square values of the random coefficients a_i. For a piston-removed phase, the tilt modes Z_2 and Z_3 are the major contributors to the mean-square phase value (over 86%). If it is possible to use adaptive optics techniques to remove the first N Zernike modes in the wave front, the residual phase can be represented by the expression

$$\Phi_N(2\rho/D_G, \theta) = \Phi(2\rho/D_G, \theta) - \sum_{i=1}^{N} a_i Z_i(2\rho/D_G, \theta), \tag{73}$$

and, consequently, the *mean-square phase error* for the residual phase becomes

$$\varepsilon_N^2 = \varepsilon^2 - \sum_{i=1}^{N} \langle (a_i)^2 \rangle = \sum_{i=N+1}^{\infty} \langle (a_i)^2 \rangle. \tag{74}$$

A good imaging system in the presence of atmospheric turbulence can be defined as one in which the mean square error $\varepsilon_N^2 \ll 1$.

14.5.3 Aperture filter functions

In the analysis of optical wave propagation through atmospheric turbulence, the statistical quantities of interest are often calculated for a single point in the transverse plane of a receiving aperture (e.g., all results in Chaps. 6–9 are for a single point). One way to include the finite size of the receiver aperture in the analysis is by the use of an "aperture filter function." Basically, this means that we formulate the effect of a finite receiver aperture in terms of wave number (m^{-1}) instead of physical spatial distance (m). The relation between the wave number space and the actual physical space is the two-dimensional Fourier transform.

For adaptive optics systems, the use of aperture filter functions can be particularly effective in the theoretical analysis of lower-order aberrations like piston and tilt. Below we will first derive these lower-order filter functions for an aperture of unit radius and then generalize to apertures of arbitrary size. The two-dimensional Fourier transform of the Zernike polynomials (67), scaled by the area of the aperture, is given by

$$\begin{aligned} G_i(\kappa, \phi) &= \frac{1}{\pi} \int_{-\infty}^{\infty} \int_{-\infty}^{\infty} e^{i\mathbf{r}\cdot\boldsymbol{\kappa}} Z_i(r, \theta) U(1 - |r|)\, dx\, dy \\ &= \frac{1}{\pi} \int_0^1 \int_0^{2\pi} e^{ir\kappa\cos(\theta - \phi)} Z_i(r, \theta) r\, d\theta\, dr, \end{aligned} \tag{75}$$

where $\mathbf{r} = \langle x, y \rangle$ and $\boldsymbol{\kappa} = \langle \kappa_x, \kappa_y \rangle$ are two-dimensional vectors in the spatial and wave number domains, respectively, $U(x)$ is the step function depicting the finite size of the aperture (unit radius), and in the last step we introduced the polar coordinates

$$\begin{aligned} x &= r\cos\theta, \qquad y = r\sin\theta, \\ \kappa_x &= \kappa\cos\phi, \qquad \kappa_y = \kappa\sin\phi. \end{aligned} \tag{76}$$

If we substitute the Zernike polynomials (67) directly into (75), we are led to three types of filter function described by

$$\begin{Bmatrix} G_i(\kappa) \\ G_{i,\,\text{even}}(\kappa,\,\phi) \\ G_{i,\,\text{odd}}(\kappa,\,\phi) \end{Bmatrix} = \frac{\sqrt{n+1}}{\pi} \int_0^1 \int_0^{2\pi} e^{i\kappa r \cos(\theta-\phi)} r R_n^m(r) \begin{Bmatrix} 1 \\ \sqrt{2}\cos m\theta \\ \sqrt{2}\sin m\theta \end{Bmatrix} d\theta\, dr. \quad (77)$$

Integrals of the type (77) are somewhat difficult to evaluate in general, but can be readily evaluated for some of the lower-order Zernike modes. For example, in the case of piston in which $m = 0$ and $R_0^0(r) = 1$, i.e., $Z_1[0, 0] = 1$, the above integral reduces to

$$G_1(\kappa) = \frac{1}{\pi} \int_0^1 r \int_0^{2\pi} e^{i\kappa r \cos(\theta-\phi)} d\theta\, dr = 2 \int_0^1 r J_0(\kappa r)\, dr, \quad (78)$$

from which we readily obtain

$$G_1(\kappa) = \frac{2J_1(\kappa)}{\kappa}. \quad (79)$$

For the case of tilt corresponding to $Z_2[1, 1] = 2r\cos\theta$, we find that (77) becomes

$$G_{2,\,\text{even}}(\kappa, \phi) = \frac{2}{\pi} \int_0^1 r^2 \int_0^{2\pi} e^{i\kappa r \cos(\theta-\phi)} \cos\theta\, d\theta\, dr. \quad (80)$$

To evaluate the inside integral, we use the identity (BJ3) in Appendix I written as

$$e^{i\kappa r \cos(\theta-\phi)} = J_0(\kappa r) + 2 \sum_{k=0}^{\infty} i^k J_k(\kappa r) \cos k(\theta - \phi), \quad (81)$$

which leads to

$$\begin{aligned} \int_0^{2\pi} e^{i\kappa r \cos(\theta-\phi)} \cos\theta\, d\theta = J_0(\kappa r) \int_0^{2\pi} \cos\theta\, d\theta \\ + 2\cos k\phi \sum_{k=1}^{\infty} i^k J_k(\kappa r) \int_0^{2\pi} \cos k\theta \cos\theta\, d\theta \\ + 2\sin k\phi \sum_{k=1}^{\infty} i^k J_k(\kappa r) \int_0^{2\pi} \sin k\theta \cos\theta\, d\theta. \end{aligned} \quad (82)$$

Except for the term $k = 1$ in the first summation, all other integrals above go to zero because of the orthogonality property of the trigonometric functions. Hence, we are left with

$$\begin{aligned} \int_0^{2\pi} e^{i\kappa r \cos(\theta-\phi)} \cos\theta\, d\theta &= 2i J_1(\kappa r) \cos\phi \int_0^{2\pi} \cos^2\theta\, d\theta \\ &= 2\pi i J_1(\kappa r) \cos\phi, \end{aligned} \quad (83)$$

and, consequently, the integral in (80) reduces to

$$G_{2,\,\text{even}}(\kappa,\phi) = 4i\cos\phi\int_0^1 r^2 J_1(\kappa r)\,dr = 4i\frac{J_2(\kappa)}{\kappa}\cos\phi. \tag{84}$$

Following along similar lines, it has been shown that the aperture filter functions in the general case are given by

$$\left.\begin{matrix} G_i(\kappa) \\ G_{i,\,\text{even}}(\kappa,\phi) \\ G_{i,\,\text{odd}}(\kappa,\phi) \end{matrix}\right\} = \sqrt{n+1}\,\frac{2J_{n+1}(\kappa)}{\kappa}\left\{\begin{matrix} (-1)^{n/2} \\ (-1)^{(n-m)/2}\sqrt{2}i^m\cos m\phi \\ (-1)^{(n-m)/2}\sqrt{2}i^m\sin m\phi. \end{matrix}\right. \tag{85}$$

Because of the presence of the term i^m, the filter functions (85) are sometimes called the *complex filter functions.* In practice, it is often the absolute value squared of these expressions that we want, called simply the *filter functions.* Thus, the filter functions $F(\kappa) = |G(\kappa)|^2$ are defined by

$$\left.\begin{matrix} F_i(\kappa) \\ F_{i,\,\text{even}}(\kappa,\phi) \\ F_{i,\,\text{odd}}(\kappa,\phi) \end{matrix}\right\} = (n+1)\left[\frac{2J_{n+1}(\kappa)}{\kappa}\right]^2\left\{\begin{matrix} 1(m=0) \\ 2\cos^2 m\phi \\ 2\sin^2 m\phi. \end{matrix}\right. \tag{86}$$

The above results are based on an aperture of unit radius. To account for an aperture of diameter D_G, we can make the change of variable $r = 2\rho/D_G$ in the definition of the Zernike polynomials or, alternatively, we can simply replace κ in Eqs. (85) and (86) with $\kappa D_G/2$. Also, these results are based on an infinite plane wave for the optical field. The corresponding filters for a general Gaussian-beam wave arise by the simple replacement of κ in Eqs. (85) and (86) with $\gamma\kappa D_G/2$ [21], where (see Chap. 6)

$$\gamma = 1 - (\bar{\Theta} + i\Lambda)(1 - z/L). \tag{87}$$

14.5.4 Piston and tilt removed phase variance

For a simple illustration of the use of the above filter functions, we consider the cases of phase variance over an aperture of diameter D_G with the piston and Zernike tilt removed. Such relations provide a rudimentary analysis of the performance of an optical system.

Because the use of Zernike polynomials above is based on the wave front (or the *eikonal*) Φ of the optical wave rather than on the phase S, it is necessary to multiply the eikonal by the wavenumber k to obtain the phase, i.e., $S = k\Phi$. However, because of this small difference, it is customary to also refer to the eikonal as phase. The phase variance of an infinite plane wave at a point was discussed in Section 8.6. In particular, under a geometrical optics approximation along a slant path, it is given by

$$\begin{aligned}\sigma^2_{S,\,\mathrm{pl}}(L) &= 4\pi^2 k^2 \int_0^L \int_0^\infty \kappa \Phi_n(\kappa, z)\, d\kappa\, dz \\ &= 1.83 \left(\frac{L_0}{r_0}\right)^{5/3},\end{aligned} \tag{88}$$

where $\Phi_n(\kappa)$ is the atmospheric power spectrum, L_0 is the outer scale of turbulence, and r_0 is Fried's parameter. In evaluating the integral in (88), we have used the von Kármán spectrum (Section 3.3.2). Clearly, for $r_0 \ll L_0$, the phase variance becomes quite large.

The piston filter function corresponds to $F_i(\kappa)$ in (86) in which $m = n = 0$. When piston is removed from the phase fluctuations over an aperture, the resulting *piston-removed phase variance* is

$$\sigma^2_{S,\,\mathrm{pl}}(L) = 4\pi^2 k^2 \int_0^L \int_0^\infty \kappa \Phi_n(\kappa, z) \left\{ 1 - \left[\frac{2J_1(\kappa D_G/2)}{\kappa D_G/2} \right]^2 \right\} d\kappa\, dz. \tag{89}$$

The original integral in (88) diverges for a simple Kolmogorov spectrum and, therefore, must be analyzed with a spectrum containing an outer scale parameter such as the von Kármán spectrum. However, because the filter function in (89) appears as a difference, the singularity in the Kolmogorov spectrum at the origin will have a canceling effect on these terms and the integral converges to [21]

$$\sigma^2_{S,\,\mathrm{pl}}(L) = 1.03 \left(\frac{D_G}{r_0}\right)^{5/3}. \tag{90}$$

For the sake of comparison, we note that by using the *ABCD* ray-matrix technique presented in Chap. 10 for aperture averaging, the piston-removed phase variance leads to

$$\begin{aligned}\sigma^2_{S,\,\mathrm{pl}}(L) &= 4\pi^2 k^2 \int_0^L \int_0^\infty \kappa \Phi_n(\kappa, z) \left[1 - \exp\left(-\frac{\kappa^2 D_G^2}{16} \right) \right] d\kappa\, dz \\ &= 1.02 \left(\frac{D_G}{r_0}\right)^{5/3},\end{aligned} \tag{91}$$

virtually the same result as (90).

The *tilt phase variance* averaged over the receiver aperture requires the filter function (86) with $m = n = 1$, from which we obtain

$$\sigma^2_{S,\,\mathrm{pl}}(L) = 64\pi^2 k^2 \int_0^L \int_0^\infty \kappa \Phi_n(\kappa, z) \left[\frac{J_2(\kappa D_G/2)}{\kappa D_G/2} \right]^2 d\kappa\, dz. \tag{92}$$

The evaluation of this integral yields [21]

$$\sigma^2_{S,\,\mathrm{pl}}(L) = 0.90 \left(\frac{D_G}{r_0}\right)^{5/3}. \tag{93}$$

The difference between (90) and (93) gives us the *phase variance with piston and tilt removed*, viz.,

$$\sigma^2_{S,\,\mathrm{pl}}(L) = 0.13\left(\frac{D_G}{r_0}\right)^{5/3}. \tag{94}$$

14.6 Summary and Discussion

Image degradation due to optical turbulence causes *image blurring* and *image dancing*, among other effects. Several related statistical parameters are commonly used to quantify the performance characteristics of an imaging system that operates in the open atmosphere. These parameters include the *point spread function* (PSF), the *optical transfer function* (OTF) of the optical system and atmospheric effects, and the *Strehl ratio* (SR). The PSF is the image-plane irradiance distribution that results from imaging a point source. The width of the main lobe of the PSF gives some indication of the resolution of the imaging system. The PSF and OTF are directly related through two-dimensional Fourier transform pairs. The modulus of the OTF is known as the *modulation transfer function* (MTF). Because the MTF of the optical wave is dominated by phase fluctuations, it is often approximated by the overall MTF obtained from the mutual coherence function. Finally, the Strehl ratio is determined by comparing the peak of the main lobe of the PSF with that of an unaberrated system.

Owing to the deleterious effects of optical turbulence on an imaging system, compensation methods like *adaptive optics* (AO) techniques play an increasingly important role in imaging applications. In calculating the above metrics for analyzing the AO system performance, it is useful to introduce Fried = s *atmospheric coherence width* r_0 defined by

$$\text{Plane wave:}\quad r_0 = \left[0.42k^2\int_0^L C_n^2(z)\,dz\right]^{-3/5}, \tag{95}$$

$$\text{Spherical wave:}\quad r_0 = \left[0.42k^2\int_0^L C_n^2(z)z^{5/3}dz\right]^{-3/5}. \tag{96}$$

Fried's parameter is directly related to the transverse spatial coherence radius by $r_0 = 2.1\rho_0$. The usable field of view in utilizing a guide star for wave front correction in an AO system can be defined by the *isoplanatic angle*

$$\theta_0 = \left[2.91k^2\int_0^L C_n^2(z)z^{5/3}dz\right]^{-3/5}. \tag{97}$$

The *Greenwood time constant*, which specifies the time interval over which wind-driven optical turbulence remains essentially unchanged, is

$$\tau_0 = \left[2.91k^2 \int_0^L C_n^2(z) V^{5/3}(z)\, dz\right]^{-3/5}, \tag{98}$$

where $V(z)$ is the wind velocity (speed) as a function of propagation distance.

In terms of Fried's parameter, the *turbulence MTF* takes the form

$$\mathrm{MTF}_{\mathrm{turb}}(\nu) = \exp\left[-3.44\left(\frac{\lambda F_G \nu}{r_0}\right)^{5/3}\right], \quad 1/L_0 \ll \nu \ll 1/l_0, \tag{99}$$

where F_G is the focal length of the collecting lens. The turbulence MTF provides a measure of the highest spatial frequency observed in the imaging system. In particular, by calculating the volume under the total MTF [combining (99) with the MTF of the optics alone], we are led to the *long-exposure resolution*

$$\frac{R}{R_{\max}} \cong \frac{(D_G/r_0)^2}{\left[1 + (D_G/r_0)^{5/3}\right]^{6/5}} \sim \begin{cases} (D_G/r_0)^2, & D_G \ll r_0, \\ 1, & D_G \gg r_0. \end{cases} \tag{100}$$

The asymptotic form of (100) for large apertures D_G illustrates the limiting resolution obtained from an optical system in the presence of optical turbulence. Again using Fried's parameter with the PSF, we can determine the *Strehl ratio*

$$\mathrm{SR} = \frac{\mathrm{PSF}(0)}{\mathrm{PSF}_0(0)} \cong \frac{1}{\left[1 + (D_G/r_0)^{5/3}\right]^{6/5}}. \tag{101}$$

Last, we find that in analyzing the effects of optical turbulence on an imaging system, it is useful to represent the corrupted phase in a series of orthogonal polynomials known as the *Zernike polynomials.* Lower-order Zernike polynomials represent such aberrations as *piston*, *tilt*, *focus*, *astigmatism*, and *coma.*

14.7 Worked Examples

Example 1: Consider an unresolved target located at range 5 km. If a lidar imaging system uses a spherical wave to illuminate the target and operates in a bistatic configuration at wavelength $\lambda = 1.06\ \mu\mathrm{m}$ and $C_n^2 = 2 \times 10^{-13}\ \mathrm{m}^{-2/3}$, calculate the following (see also Example 2 in Chap. 13):

(*a*) Fried's parameter for calculating the turbulence MTF.
(*b*) The on-axis scintillation index of the echo wave in the receiver plane.
(*c*) What is the scintillation index on the detector if the receiver aperture is 10 cm?
(*d*) What is the residual scintillation index for a very large receiver aperture?

(*e*) If the SNR in free space is $\text{SNR}_0 = 30$ dB, what is the corresponding mean SNR for a shot-noise limited system, assuming the receiver aperture is 10 cm?

Solution: We first calculate the quantities:

$$\sigma_R^2 = 1.23 C_n^2 k^{7/6} L^{11/6} = 118.6, \quad \beta_0^2 = 0.5 C_n^2 k^{7/6} L^{11/6} = 48.21$$

$$d_G^2 = \frac{k D_G^2}{4L} = 2.96$$

(*a*) Because the index of refraction structure parameter is constant, we use the spherical wave expression

$$r_0 = \left(0.16 C_n^2 k^2 L^{11/6}\right)^{-3/5} = 0.56\,\text{cm}.$$

(*b*) From Eq. (51) with $D_G = 0$, we find $\sigma_I^2(0, 2L + L_f)_{\text{bistatic}} = 4.90$.

(*c*) From Eq. (51) with $D_G = 10\,\text{cm}$, we find $\sigma_I^2(D_G, 2L + L_f)_{\text{bistatic}} = 1.97$.

(*d*)

$$\lim_{D_G \to \infty} \sigma_I^2(D_G, 2L + L_f)_{\text{bistatic}}$$

$$= \exp\left[\frac{0.49\beta_0^2}{\left(1 + 0.56\beta_0^{12/5}\right)^{7/6}} + \frac{0.51\beta_0^2}{\left(1 + 0.69\beta_0^{12/5}\right)^{5/6}}\right] - 1 = 1.43.$$

(*e*)

$$\langle \text{SNR} \rangle = \frac{\text{SNR}_0}{\sqrt{1 + \sigma_I^2(D_G, 2L + L_f)\text{SNR}_0^2}} = -1.47\,\text{dB}.$$

❑

Problems

Section 14.3

1. The MTF in free space is defined by the two-dimensional Fourier transform

$$\mathrm{MTF}_0(\nu) = C\int\!\!\int_{-\infty}^{\infty} I^0(r,L)e^{2\pi i\boldsymbol{\nu}\cdot\mathbf{r}}d^2r,$$

where C is a normalization constant. From the PSF defined by Eq. (16), show that $C = 16/\pi D_G^2$ and deduce the result given by

$$\mathrm{MTF}_0(\nu) \cong \exp\left[-4\left(\frac{\lambda L_f \nu}{D_G}\right)^2\right].$$

2. Given the mean irradiance [see Eq. (45) in Chap. 10]

$$\langle I(\mathbf{r}, L+L_f)\rangle = \frac{W_G^2}{W^2}\exp\left(-\frac{2r^2}{W^2}\right)\exp\left\{-4\pi^2k^2L\int_0^1\int_0^\infty \kappa\Phi_n(\kappa) \times\left[1-\exp\left(\frac{L\kappa^2\xi^2}{k\Omega_G}\right)I_0\left(\frac{2\kappa\xi Lr}{L_f\Omega_G}\right)\right]d\kappa\, d\xi\right\},$$

(*a*) show that the on-axis mean irradiance can be approximated by ($W = 2L_f/kW_G^2$)

$$\langle I(0, L+L_f)\rangle = \mathrm{PSF}(0) = \frac{\pi^2 D_G^4}{64\lambda^2 L_f^2\left[1+(D_G/r_0)^{5/3}\right]}.$$

Hint: Use the approximation $\exp(-T) \cong 1/(1+T)$.

(*b*) Write the bracket term in the mean irradiance given above in the form

$$1-\exp\left(-\frac{L\kappa^2\xi^2}{k\Omega_G}\right)I_0\left(\frac{2\kappa\xi Lr}{L_f\Omega_G}\right) = \left[1-\exp\left(-\frac{L\kappa^2\xi^2}{k\Omega_G}\right)\right] \times\exp\left(-\frac{L\kappa^2\xi^2}{k\Omega_G}\right)\left[1-I_0\left(\frac{2\kappa\xi Lr}{L_f\Omega_G}\right)\right],$$

where the first term on the right produces the result in part (*a*). Then, use the approximation given in (44) of Chap. 6 to deduce that

$$\mathrm{PSF}(\mathbf{r}) = \frac{\pi^2 D_G^4}{64\lambda^2 L_f^2\left[1+(D_G/r_0)^{5/3}\right]}\exp\left\{-\frac{\pi^2 D_G^2 r^2}{4\lambda^2 L_f^2[1+(D_G/r_0)^{5/3}]}\right\}.$$

3. Show that the normalized two-dimensional Fourier transform of the PSF given in Prob. 2 leads to

$$\mathrm{MTF}_{\mathrm{total}}(\nu) = \exp\left[-4\left(\frac{\lambda L_f\nu}{D_G}\right)^2\right]\exp\left[-4\left(\frac{\lambda L_f\nu}{D_G}\right)^{1/3}\left(\frac{\lambda L_f\nu}{r_0}\right)^{5/3}\right].$$

4. In the absence of atmospheric turbulence the long exposure resolution (29) reduces to

$$R = \frac{4D_G^2}{\lambda^2 F_G^2}\int_0^1 u\Big(\cos^{-1} u - u\sqrt{1-u^2}\Big)\,du.$$

(*a*) Use the integral formula

$$\int_0^1 u\Big(\cos^{-1} u - u\sqrt{1-u^2}\Big)\,du = \frac{\pi}{16}$$

to deduce that the resolution becomes $R = \pi D_G^2/4\lambda^2 F_G^2$.

(*b*) Show that the implied resolution from the MTF (18) is also $R = \pi D_G^2/4\lambda^2 F_G^2$.

5. Use Eq. (29) to show that

$$R_{\max} = \lim_{D_G\to\infty} R = \frac{\pi r_0^2}{4\lambda^2 F_G^2}.$$

6. With $R_{\max} = \pi r_0^2/4\lambda^2 F_G^2$ from Prob. 5, we can rewrite the normalized long exposure resolution as

$$\frac{R}{R_{\max}} = \frac{16}{\pi}\left(\frac{D_G}{r_0}\right)^2\int_0^1 u\Big[\cos^{-1} u - u\sqrt{1-u^2}\Big]\exp\left[-3.44\left(\frac{D_G u}{r_0}\right)^{5/3}\right]du.$$

(*a*) For $D_G \ll r_0$, deduce that

$$\frac{R}{R_{\max}} \sim \left(\frac{D_G}{r_0}\right)^2, \quad D_G \ll r_0.$$

(*b*) Show that the change of variable $t = (Du/r_0)^{5/3}$ in the above integral results in the expression

$$\frac{R}{R_{\max}} = \frac{48}{5\pi}\int_0^{(D_G/r_0)^{3/5}} t^{1/5}\left\{\cos^{-1}\left(\frac{r_0 t^{3/5}}{D_G}\right) - \frac{r_0 t^{3/5}}{D_G}\left[1-\left(\frac{r_0 t^{3/5}}{D_G}\right)^2\right]^{1/2}\right\}e^{-3.44t}dt.$$

(*c*) For $D_G \gg r_0$, use the integral in (*b*) to deduce the asymptotic result

$$\frac{R}{R_{\max}} \sim \frac{24}{5}\int_0^\infty t^{1/5}e^{-3.44t}dt = 1.$$

7. Given the tilt-removed PSF (31), set $r = 0$ and

(*a*) show that it reduces to

$$\mathrm{PSF}_{\mathrm{ST}}(0) = \frac{\pi^2 D_G^4}{64\lambda^2 L_f^2\big[1 + 0.28(D_G/r_0)^{5/3}\big]}.$$

(*b*) Use the technique in Prob. 2(*b*) to deduce in general that

$$\mathrm{PSF}_{\mathrm{ST}}(\mathbf{r}) = \frac{\pi^2 D_G^4}{64\lambda^2 L_f^2[1 + 0.28(D_G/r_0)^{5/3}]} \times \exp\left\{-\frac{\pi^2 D_G^2 r^2}{4\lambda^2 L_f^2[1 + 0.28(D_G/r_0)^{5/3}]}\right\}.$$

Section 14.4

8. For Example 1,
   (*a*) what is the scintillation index (flux variance) on the detector if the receiver aperture is increased to 40 cm?
   (*b*) What is the corresponding mean signal-to-noise ratio if $\mathrm{SNR}_0 = 50$ dB?
9. For Example 1,
   (*a*) What is the scintillation index (flux variance) on the detector if the path length is 1 km, $C_n^2 = 2 \times 10^{-14}\,\mathrm{m}^{-2/3}$, and the receiver aperture is 40 cm?
   (*b*) What is the corresponding mean signal-to-noise ratio if $\mathrm{SNR}_0 = 50$ dB?
10. Given the conditions in Prob. 9(*a*), what is the maximum mean SNR possible given that SNR_0 can be as large as desired?

Section 14.5

11. For the radial polynomials (58) of the Zernike set,
   (*a*) show that

$$R_n^m(r) = n!\left(\frac{n-m}{2}\right)!\left(\frac{n+m}{2}\right)! \times {}_2F_1\left(-\frac{n-m}{2}, -\frac{n+m}{2}; -n; \frac{1}{r^2}\right).$$

   (*b*) From part (*a*), verify that $R_n^m(1) = 1$.
12. Follow the technique in Section 14.5 used for evaluating $G_{2,\mathrm{even}}(\kappa, \phi)$ (corresponding to $Z_2[1,1]$) to deduce that (corresponding to $Z_3[1,1]$)
   (*a*)

$$G_{3,\mathrm{odd}}(\kappa, \phi) = 4i\frac{2J_2(\kappa)}{\kappa}\sin\phi.$$

   (*b*) Corresponding to the Zernike function $Z_4[0,2]$, calculate the filter function $G_{4,\mathrm{even}}(\kappa, \phi)$.

References

1. D. L. Fried, "Optical resolution through a randomly inhomogeneous medium," *J. Opt. Soc. Am.* **56**, 1372–1379 (1966).
2. F. Roddier, "The effects of atmospheric turbulence in optical astronomy," in *Progress in Optics XIX*, E. Wolf, ed. (North Holland, New York, 1981).
3. M. C. Roggeman and B. Welsh, *Imaging Through Turbulence* (CRC Press, Boca Raton, 1996).
4. *Selective Papers on Adaptive Optics for Atmospheric Compensation*, J. E. Pearson, ed., SPIE Milestone Series MS-92 (SPIE Optical Engineering Press, Bellingham, Wash., 1994).
5. D. L. Fried, "Anisoplanatism in adaptive optics," *J. Opt. Soc. Am.* **72**, 15–61 (1982).
6. D. Dravens, L. Lindgren, E. Mezey, and A. T. Young, "Atmospheric intensity scintillation of stars: I. Statistical distributions and temporal properties," *Proc. Astron. Soc. of the Pacific* **109**, 173–207 (1997); "Atmospheric intensity scintillation of stars: II. Dependence of optical wavelength," *Proc. Astron. Soc. of the Pacific* **109**, 725–737 (1997); "Atmospheric intensity scintillation of stars: III. Effects for different telescope apertures," *Proc. Astron. Soc. of the Pacific* **110**, 610–633 (1998); Erratum: *Proc. Astron. Soc. of the Pacific* **110**, 1118 (1998).
7. R. L. Fante, "Imaging of an object behind a random phase screen using light of arbitrary coherence," *J. Opt. Soc. Am. A* **2**, 2318–2329 (1985).
8. V. U. Zavarotnyi, "Imaging of an object behind a random phase screen using light of arbitrary coherence: comment," *J. Opt. Soc. Am. A* **5**, 263–264 (1988).
9. R. L. Fante, "Imaging of an object behind a random phase screen using light of arbitrary coherence: reply to comment," *J. Opt. Soc. Am. A* **5**, 265 (1988).
10. T. Mavroidis, C. J. Solomon, and J. C. Dainty, "Imaging a coherently illuminated object after double passage through a random screen," *J. Opt. Soc. Am. A* **8**, 1003–1013 (1991).
11. M. Wellfare, T. Holmes, S. Pohlman, D. Geci, K. Norris-Zachery, and R. Patton, "Identification of vehicle targets from low-cost ladar seeker imagery," in *Laser Radar Technology and Applications*, G. W. Kammerman, ed., Proc. SPIE **2748**, 272–282 (1996).
12. J. W. Goodman, *Introduction to Fourier Optics* (McGraw-Hill, New York, 1968).
13. J. D. Gaskill, *Linear Systems, Fourier Transforms, and Optics* (Wiley & Sons, New York, 1978).
14. J. W. Goodman, *Statistical Optics* (Wiley & Sons, New York, 1985).
15. M. Born and E. Wolf, *Principles of Optics*, 7th ed. (Cambridge University Press, Cambridge, 1999).
16. B. A. Saleh and M. C. Teich, *Fundamentals of Photonics* (John Wiley & Sons, New York, 1991).
17. N. S. Kopeika, *A System Engineering Approach to Imaging* (SPIE Optical Engineering Press, Bellingham, Wash., 1998).

18. R. G. Driggers, P. Cox, and T. Edwards, *Introduction to Infrared and Electro-Optical Systems* (Artech House, Boston, 1999).
19. D. L. Fried, "Optical heterodyne detection of an atmospherically distorted signal wave front," *Proc. IEEE* **55**, 57–67 (1967).
20. D. P. Greenwood, "Bandwidth specifications for adaptive optics systems," *J. Opt. Soc. Am.* **67**, 390–392 (1977).
21. R. J. Sasiela, *Electromagnetic Wave Propagation in Turbulence* (Springer, New York, 1994).
22. L. C. Andrews, *Special Functions of Mathematics for Engineers*, 2nd ed. (SPIE Optical Engineering Press, Bellingham, Wash.; Oxford University Press, Oxford, 1998); [formerly published as 2nd ed. by McGraw-Hill, New York (1992)].
23. J. H. Shapiro, B. A. Capron, R. C. Harney, "Imaging and target detection with a heterodyne-reception optical radar," *Appl. Opt.* **20**, 3292–3313 (1981).
24. G. W. Kamerman, ed., *Selected Papers on Laser Radar*, SPIE Milestone Series, Vol. MS 133 (SPIE Optical Engineering Press, Bellingham, Wash., 1997).
25. L. C. Andrews, R. L. Phillips, and C. Y. Hopen, *Laser Beam Scintillation with Applications* (SPIE Optical Engineering Press, Bellingham, Wash., 2001).
26. R. J. Noll, "Zernike polynomials and atmospheric turbulence," *J. Opt. Soc. Am.* **73**, 207–211 (1976).
27. R. K. Tyson, *Principles of Adaptive Optics* (Academic Press, San Diego, 1991).